Visual Abstract

Analysis of the resistance to crack propagation in SENT test specimens printed in ABS using parallel or crossed filaments between layers

O. Aourik, A. Chouaf, M. Othmani

Hassan II University, National School of Electricity and Mechanics, Casablanca, Morocco
oumaima.aourik@ensem.ac.ma, http://orcid.org/0000-0002-7451-5213
a.chouaf@ensem.ac.ma, http://orcid.org/0000-0003-1765-6762
mourad.othmani@ensem.ac.ma, http://orcid.org/0000-0001-8601-8073

ABSTRACT. Additive manufacturing techniques continue to develop and cover all industrial fields. However, the performances of aspect and mechanical behavior of the parts obtained by this process remain to be mastered and are still the subject of current research works. Among these performances, the one corresponding to the resistance to the propagation of cracks. In order to improve this very interesting property in various industrial fields, it is desirable to master the understanding of crack propagation in this type of structure obtained by 3D printing. The objective of this paper is to analyze and understand the effect of the adopted raster angle on the crack propagation in SENT specimens obtained by FDM in ABS (Acrylonitrile-Butadiene-Styrene). Two approaches were developed: one is experimental to determine the critical stress intensity factor K_{IC} and the other is numerical to predict the possible paths of crack propagation.

KEYWORDS. Additive Manufacturing, FDM, Raster Angle, ABS, Crack, Numerical Simulation.

OPEN ACCESS

INTRODUCTION

Over the past decade, additive manufacturing (AM) has attracted considerable attention in the development and manufacturing industries. We can mention the medical, engineering, aerospace, and automotive fields [1-4]. Despite the progress that additive manufacturing methods are experiencing, in addition to significant technological and material advances, the quality of printed objects still needs to be improved. Indeed, by this process, which involves many manufacturing parameters, it is very difficult to obtain a part with the desired mechanical performance. This is due to the lack of control of the multi-physical interactions of these parameters [5-12].

Given the complexity of the problem, it is essential to make an optimal choice of a particular permutation of these parameters for a given performance. It is in this sense that many researchers have developed their studies on the qualities of printed parts. Among these works is that of Turner et al, who addressed the relationship between printing parameters

and the dimensional and surface properties of finished parts [13]. Lubombo et al. examined the influence of the type of filling pattern on the stiffness and strength of 3D printed PLA parts [14]. In parallel to these studies, a numerical approach was conducted by Othmani et al. to improve the meso-structural modeling of a tensile specimen obtained virtually by FDM [15]. This modeling made it possible to simulate by the finite element method the mechanical behavior of the parts obtained by FDM in ABS. Through the results of the study by Othmani et al., we were able to correlate the choice of parameters with the mechanical resistance of the part.

Among these performance issues, the mechanical behavior of printed parts is still of great interest to industry and researchers. In this regard, many studies have been developed to examine the effect of printing parameters on the mechanical performance of printed parts. The review by Sood et al. addressed the effect of five printing parameters, which are layer thickness, part build orientation, raster angle, raster width, and filament gap on the compressive strength of these parts [16].

Through all these studies, we found that the aspects of fracture behavior and crack path are not sufficiently studied, especially with regard to numerical simulations in this type of research work. Among the few works, we can cite the article by Ayatollahi et al. who confirmed that the orientation of the filament of deposited material relative to the tip of the crack seems to play the most important role in modifying the fracture toughness of printed parts [17]. The study developed by Ameri et al., focused on the effect of the raster angle on the crack path using the extended finite element method and the cohesive zone model (XFEM-CZM) [18].

Finally, this aspect of damage by crack propagation in printed parts has been little developed, especially the understanding of the mechanism generated during the process of rupture [19-25]. It is this mechanism that we have tried to highlight in the present study limited to the effect of the raster angle on the crack propagation for printed parts. For this purpose, we have developed two approaches, one is experimental and the other is numerical. From the experimental approach, we have characterized the mechanical behavior of SENT specimens made in two configurations. For the first configuration, the filaments are parallel between layers and for the second, the filaments are crossed between layers. The curves resulting from this experimental approach allowed us to determine the critical stress intensity factor (K_{IC}) for the studied cases. For the numerical approach, we performed numerical simulations of the behavior of these SENT specimens, and it is from the Von Mises stress distributions that we tried to predict the possible paths of crack propagation.

EXPERIMENTAL APPROACH

Manufacture of test specimens

In this approach, Single Edge Notch Tension (SENT) specimens (Fig. 1), were made to study the impact of several raster angles on the crack propagation resistance in printed ABS specimens.
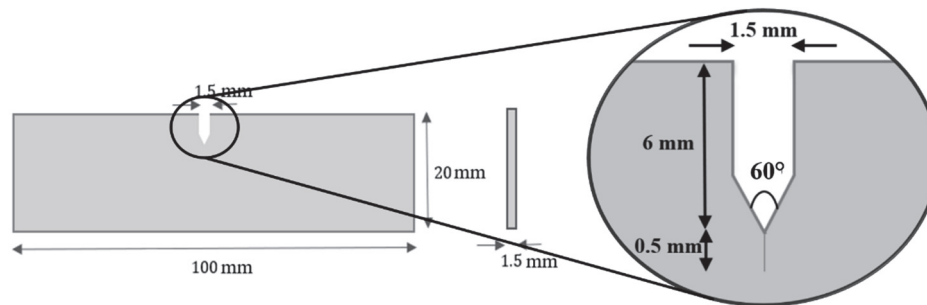

Figure 1: Dimensions of the SENT specimen ISO 13586 and ASTM D5045.

These specimens were modeled on CAD software according to ISO 13586 and ASTM D5045 [26-27]. Then, the model is converted into a Stereolithography (STL) file, which was also translated into a machine instruction file, written in G-code language describing the trajectories of the filling material. Once the file is obtained, the samples will be ready to be printed with the RAISE 3D printer using the FDM technique (Fig. 2). The notch was made during the 3D printing of the test sample. However, the pre-cracking or initiation of the crack was carried out manually with a cutter. Its depth is around 0.5 mm (see figure above). The pre-cracks were checked by profile projector.
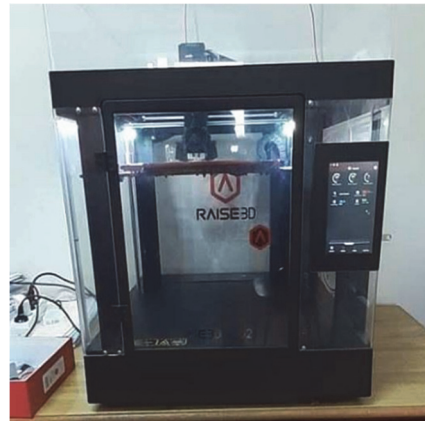
Figure 2: 3D printer used: RAISE 3D.

The parameters used to print SENT specimens are listed below in Tab. 1.

Parameters	Values	Units
Layer thickness	0.2	mm
First layer printing speed	30	mm/s
Print speed of other layers	150	mm/s
Build orientation	XYZ	
Infill percentage	100	%
Number of perimeters	2	
Temperature	230	°C

Table 1: Parameters considered for the printing of the specimens.

We recall that this FDM printing technique is a successive layer building process that allows us to control the raster's angle of each layer separately, and produce samples with different raster angles from one layer to another.

We have therefore chosen to work with two different types of specimens. The first type adopts aligned layers (parallel filaments between layers), while the second type adopts crossed layers (crossed filaments between layers). In this case, two successive layers are printed with two different angles. To realize these specimens, we have considered two configurations: For Configuration (1) the layers are aligned with raster angles of 15°, 30°, 45°, 60° and 75°. For Configuration (2) the successive layers are cross-filament with alternating raster angles (15°/-75°), (30°/-60°) and (45°/-45°) see Fig. 3.
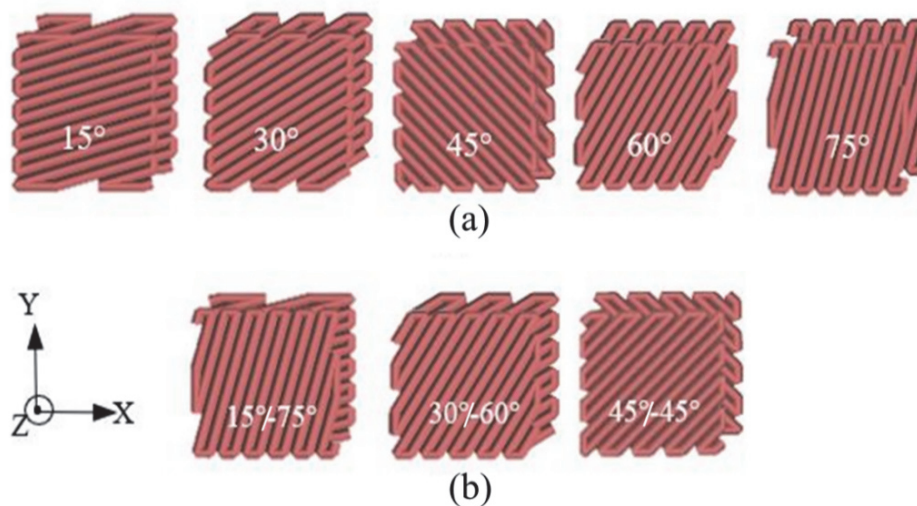

Figure 3: Raster angles used for: (a) Configuration (1): filaments are parallel between layers and (b) Configuration (2): filaments are crossed between layers.

Mechanical tests

To carry out our tensile tests on the SENT specimens for which crack initiation was introduced, we used an MTS Criterion Model 45 machine with a maximum load of 100 kN (Fig. 4).
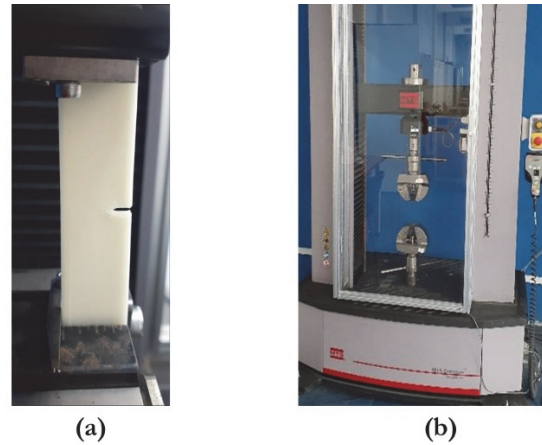

(a)   **(b)**

Figure 4: (a) SENT test specimen printed in ABS, (b) 'MTS Criterion Model 45' tensile testing device.

Results

From our tensile tests according to the standards, we obtained the stress-strain curves for the two configurations as shown in Figs. 5 and 6.

In Fig. 6, for each of the combinations studied (15°/-75°, 30°/-60°, and 45°/-45°) we have integrated the corresponding photo showing the crack propagation from the pre-crack. On the other hand, in Fig. 5, we have integrated only the corresponding photo at the angle of raster 30°, for reasons of congestion.
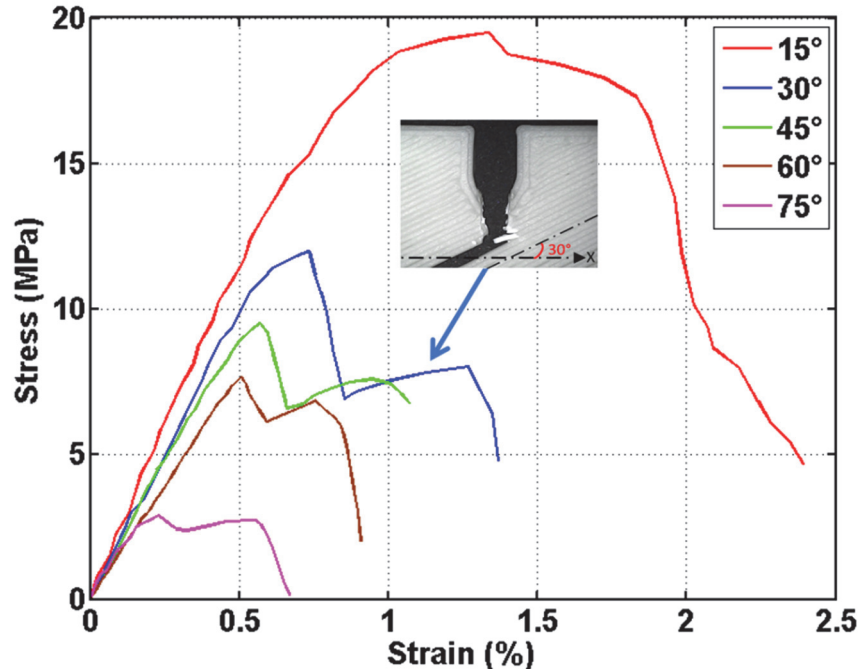

Figure 5: Stress-strain curves configuration (1): parallel filaments between layers.

According to these results, the damage mechanism for the ABS SENT samples obtained by FDM, seems to be affected by the raster angle for both configurations but to different degrees.

For configuration (1) (parallel filaments between layers), the curves show a very marked difference in the mechanical behavior between the different cases of raster angle. Indeed, the raster angle plays a significant role in the damage process

of SENT samples. When the raster angle created between the filament and the axis of the applied load is small, the tensile strength is better. This resistance decreases with the increase of the angle in a remarkable way.

For configuration (2), the curves in Fig. 6 show that the three specimens (15°/-75°; 30°/-60° and 45°/-45°) have a mechanical strength of the same order of magnitude (between 14 MPa and 15 MPa). However, the case (45°/-45°) is clearly distinguished from the other two cases by a large phase of non-linear behavior. This very marked phase could be generated by the multitude of internal bifurcations of the crack during the progressive damage of the (45°/-45°).

For the determination of the critical stress intensity factor K_{IC}, we applied the usual approach that many researchers in the field have well adopted [28].
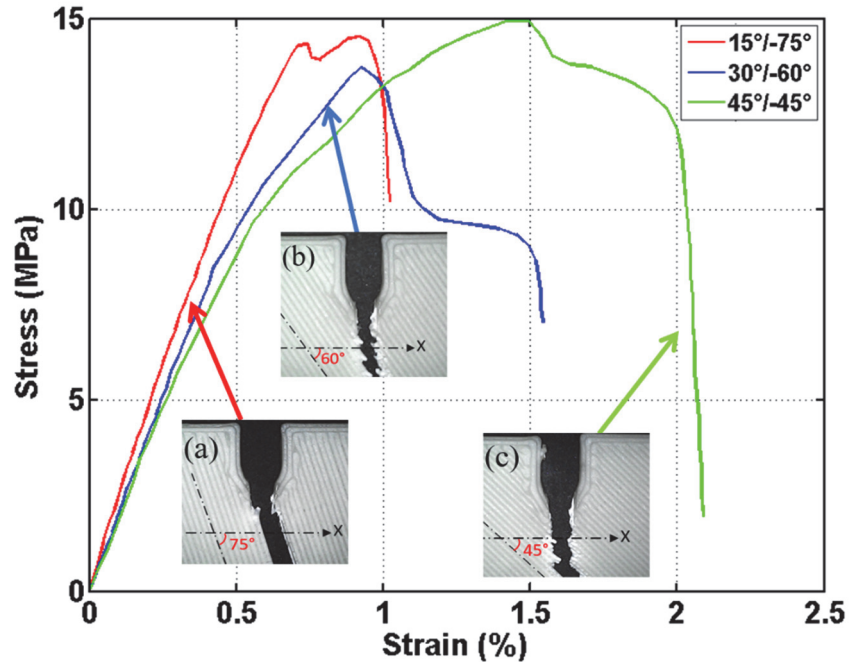

Figure 6: Stress-strain curves configuration (2): cross filaments between en layers: (a) 15°/-75°, (b) 30°/-60° and (c) 45°/-45°.

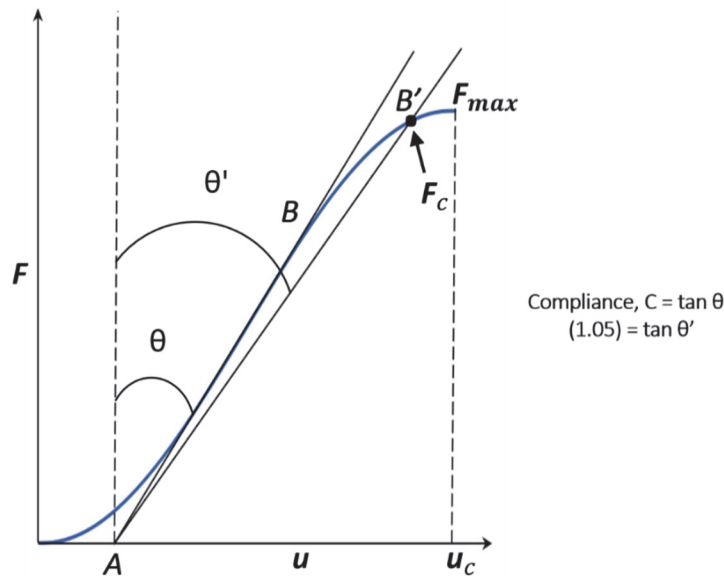Figure 7: Principle of determination of C and F_C.

To do this, we considered our Force-Displacement curves on which we drew the best straight line (AB) to determine compliance 'C', as schematically shown in Fig. 7. The value of C is given by the reciprocal of the slope of the line (AB). A second line (AB') was drawn with a compliance 5% greater than that of line (AB). If the maximum load the specimen can

support, Fmax, falls between the (AB) and (AB') lines, then Fmax is used to calculate the K$_{IC}$. If Fmax is outside of line (AB) and line (AB'), then the intersection of line (AB') and the load curve can be considered the critical load F$_C$.

It is this critical load F$_C$ that we used to calculate the critical stress σ_C by considering the net section of the specimen. Finally, from the obtained values of σ_C, we calculated those of K$_{IC}$ by the classical formula below:

$$K_{IC} = \sigma_C \sqrt{\pi a}\, f\left(\frac{a}{W}\right)$$

(1)

where σ_C is the critical stress, **a** is the notch length, **W** is the specimen width, and $f\left(\dfrac{a}{w}\right)$ is a geometric function given by:

$$f\left(\frac{a}{w}\right) = 1.12 - 0.23\left(\frac{a}{w}\right) + 10.56\left(\frac{a}{w}\right)^2 - 21.74\left(\frac{a}{w}\right)^3 + 30.42\left(\frac{a}{w}\right)^4$$

(2)

The results obtained for the two configurations studied are grouped in Tab. 2.

Configuration (1): parallel filaments between layers				
Raster angle	15°	30°	45°	60°	75°
K_{IC} ($MPa\sqrt{m}$)	3.64	2.72	2.16	1.74	0.66
Configuration (2): cross filaments between layers				
Raster angle	15°/-75°		30°/-60°		45°/-45°
K_{IC} ($MPa\sqrt{m}$)	3.31		3.13		3.41

Table 2: Critical stress intensity factors K$_{IC}$ obtained.

For the first configuration (parallel filaments between layers), when the raster angle is small, the behavior of an FDM printed ABS part approaches that of continuous ABS [29]. In the literature, authors Khatri et al. [30] were able to find a K$_{IC}$ value of 3.66 $MPa\sqrt{m}$ for an angle of 0°. This value is of the same order of magnitude as the value we found (3.64 $MPa\sqrt{m}$) for our smallest studied angle (15°). As the angle increases, the resistance to crack propagation becomes lower. For the second configuration (cross filaments between layers), the K$_{IC}$ is almost the same for the three cases studied (15°/-75°), (30°/-60°) and (45°/-45°). However, the (45°/-45°) case has a slightly higher K$_{IC}$ value than the other cases. These results are discussed in section IV.

NUMERICAL APPROACH

To better understand this notion of resistance to crack propagation in printed structures, we have performed numerical simulations of the behavior of SENT specimens. It is from the stress distributions that we will try to predict the possible trajectories of crack propagation.

Geometric model and boundary conditions

The numerical approach we adopted to simulate the mechanical behavior of our SENT specimens was developed in our laboratory by Othmani et al. (co-authors of this article) [31]. Through the imitation of the manufacturing method of the

FDM process, we created digital models of the SENT specimens using a program written in "Python" language. This program imports a G-code file generated by the "Slic3r" software. The latter imports a complete model of the specimen in STL format and cuts it into several layers and trajectories, according to the selected manufacturing parameters. The execution of the program allows the calculation code "Abaqus Standard", through a Macro, to draw the trajectories as lines. From the instructions of the numerical control written in the G code file, a section is assigned to the different paths. This allows to model the cross section of the deposited filament. This section will be generated on all the lines, thus obtaining a three-dimensional part that reproduces the structure of a printed part. To create the contact between the layers and the successive filaments, we used a 'Tie' type interaction. The mesh of the digital specimen is realized with 3D tetrahedral linear elements (C3D4).

All the steps of the procedure are summarized in the flowchart below (Fig. 8) :
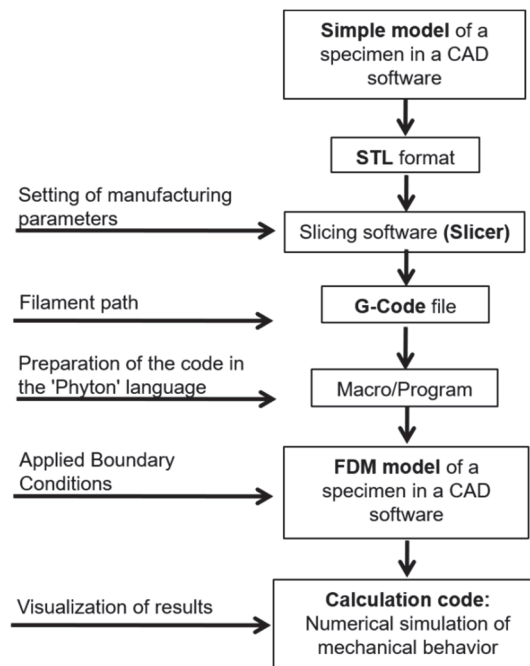

Figure 8: Steps to build the numerical samples to run the simulations

For the material used, we considered the properties of ABS filament that were obtained from the literature [32]. The values, are : 2.0 GPa for the Young's modulus, 0.3 for the Poisson's ratio and 1050 kg/m^3 for the density. The boundary conditions applied during the numerical simulation are identical to those applied during a physical test. We imposed an embedding on one face of our virtual specimen and on the other face, a forced displacement u_0 along the longitudinal axis (Fig. 9).
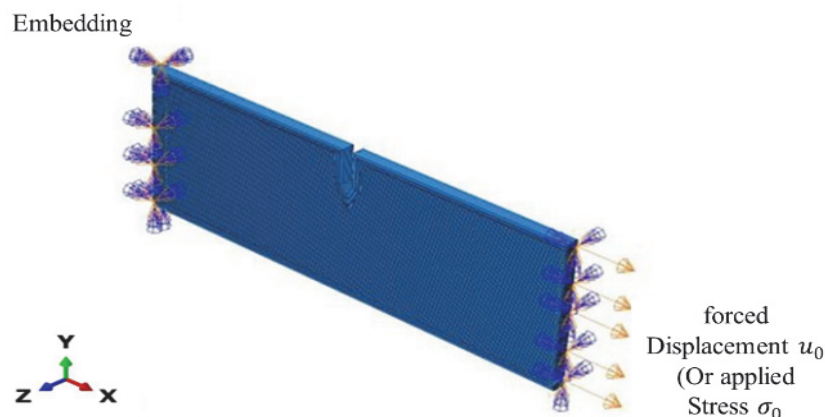

Figure 9: Geometric model of SENT specimen and boundary conditions.

Stress distribution

From the results of our simulations, we have plotted the Von Mises stress distributions for the two configurations of the printed specimens (Fig. 10).
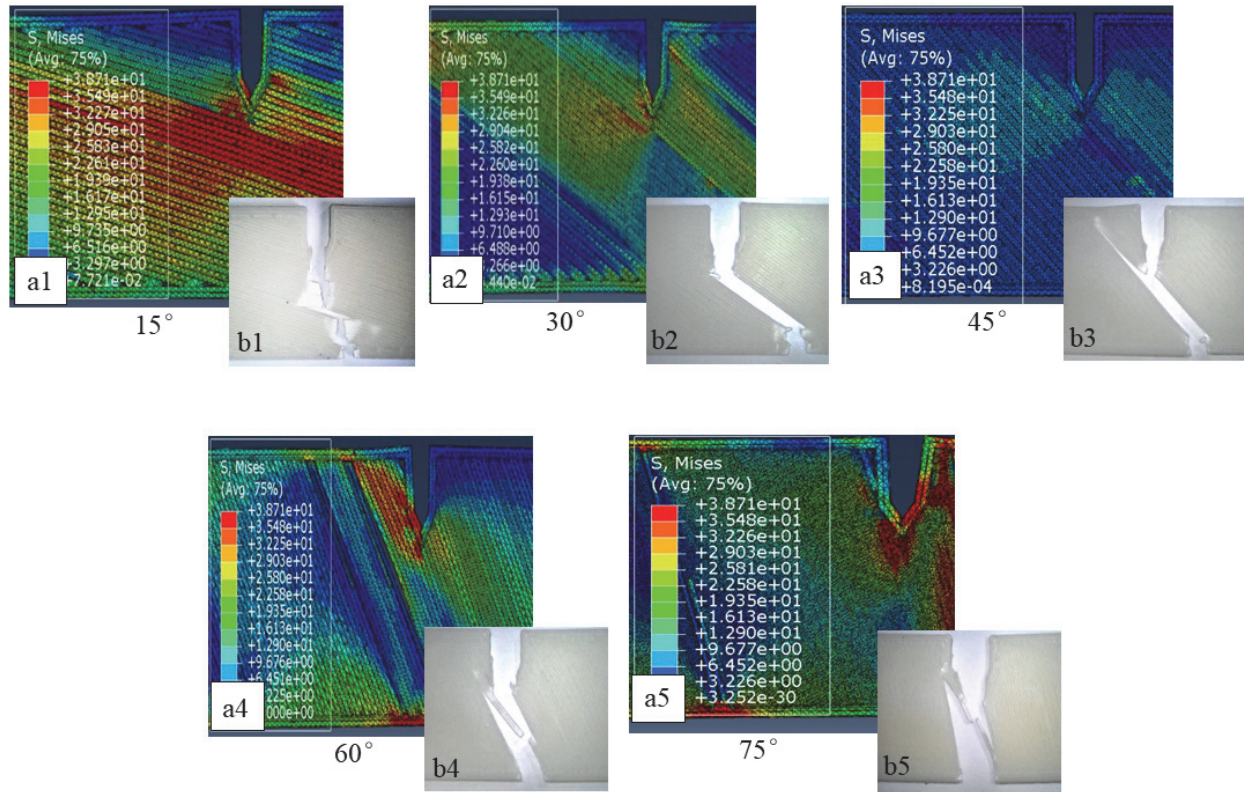

Figure 10 : (ai) Von Mises stress distribution and (bi) Damage paths for angles: (i=1) 15°, (i=2) 30°, (i=3) 45°, (i=4) 60°, (i=5) 75°.

According to these analyses, we can see for configuration (1) that the distribution of stresses highlights concentrations oriented according to the angles of the raster (Fig. 10(a1 :15°), (a2 :30°), (a3 :45°), (a4 :60°) and (a5 :75°)).

These stress concentrations are characterized by their location at the interfaces between filaments. These zones are privileged for possible crack propagation. This was confirmed by our observations (Fig. 10(b1:15°), (b2:30°), (b3:45°), (b4:60°) and (b5:75°)). Indeed, the crack initiates at the notch tip and follows a path oriented along the raster angle.

For configuration (2), which has crossed filament layers, the resistance to crack propagation is almost the same for all angle combinations, as shown by the K_{IC} values in Tab. 2. However, the crack propagation when it initiates, it follows the path of the largest angle for the cases (15°/-75°, 30°/-60°). This is because the crack easily progresses in the layers that have the weakest K_{IC} in the structure. This finding was confirmed by our observations (Fig. 11 a and b). For the case (45°/-45°), the crack propagation in the vicinity of the initiation follows the 45° angle once on the left and once on the right in a staircase form. After this localised area, the crack propagates almost straight.

Concerning this configuration 2, the numerical simulations are very complex. They are the subject of our perspectives.
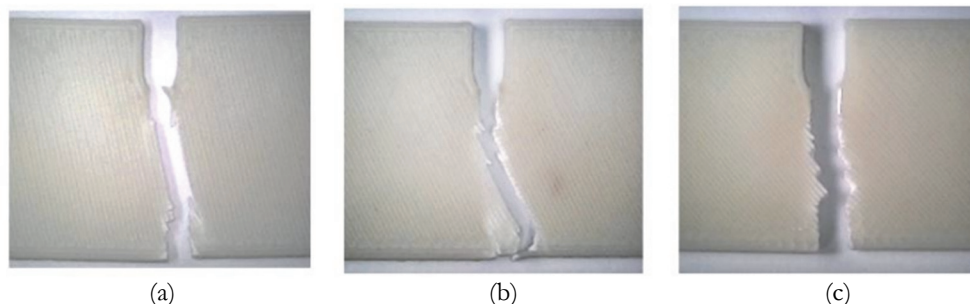

Figure 11: Macroscopic crack paths: (a) 15°/-75°, (b) 30°/-60° and (c) 45°/-45°.

DISCUSSION

To analyze the difference between the behaviors of the two configurations (1) and (2), we have deepened our observations from a digital microscope (Fig.12).
For configuration 1, the crack propagation develops between filaments following the raster angle. The fracture facies clearly show that from one layer to another, the filaments remain in the same plane (Fig. 12a). In this case, all the layers of the specimen resist the crack propagation in the same way. Depending on the raster angle, this resistance changes from one case to another. Indeed, the normal stress, which separates in mode I two adjacent filaments, is determined from the stress applied to the specimen multiplied by the sine of the raster angle. When this angle is small, the normal stress on the filament becomes small. This makes it difficult to separate the filaments. For this case, we have a better resistance. On the contrary, with the increase of the angle, the normal stress increases and can easily separate the filaments. This finding is in agreement with the values obtained by K_{IC} (Tab. 2).

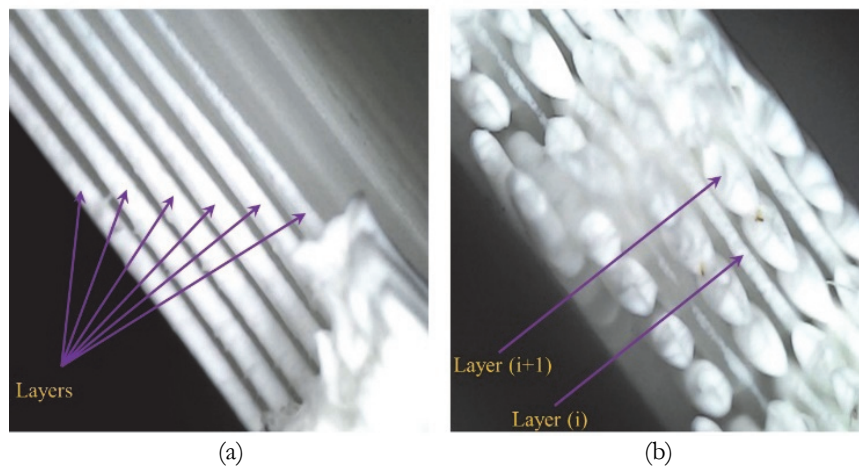(a)   (b)

Figure 12: Rupture facies: (a) Configuration (1): filaments separation and (b) Configuration (2): layer (i); filaments separation, layer (i+1); filaments rupture.

For configuration (2) with filaments crossed from one layer to the other, two types of damage can be observed (Fig. 12b). One type corresponds to filament separation and the other corresponds to transverse filament breakage. These two types of damage are alternated from one layer to the other. Indeed, the stress σ_0 applied at the end of the test piece is decomposes into tangential τi and normal σi components for a filament of a layer (i). And for the filament of layer (i+1), this stress σ_0 can be decomposed into tangential τ_{i+1} and normal σ_{i+1} components with $\tau_{i+1} = \sigma_i$ and $\sigma_{i+1} = \tau_i$. These are the components that generate the two types of damage mentioned above. The normal component to the filament generates the separation of the filaments and the tangential component, which develops longitudinally to the filament causes its rupture.
Finally, in one layer (i), we observe a damage by separation of the filaments and in the other (i+1) a transverse break of the filaments. It is this last type of damage that reveals that the resistance to crack propagation is almost identical for the different cases of configuration 2. Indeed, the filament breakage is identical for all specimens. This is why we obtained an almost identical stress intensity factor K_{IC} for the different cases of configuration 2 studied (Tab. 2).

CONCLUSION

In this contribution, the phenomenon of the breaking strength of parts obtained by 3D printing has been treated. As this phenomenon is quite complex, we limited our study to the effect of the raster angle on the propagation of the crack in a SENT specimen printed in ABS by FDM. To do this, two approaches have been developed. One is experimental to determine the K_{IC} and the other is numerical to highlight the possible paths of crack propagation in this type of structure.

From our experimental results, we determined the stress intensity factor K_{IC} for the two studied configurations. For configuration 1 (filaments parallel between layers), the K_{IC} is very sensitive to the raster angle. When the angle is small, the K_{IC} value is high, indicating good resistance to crack propagation. However, when the raster angle is large, this resistance becomes low and the damage by separation of the filaments is eminent. For this configuration, the crack propagation follows the raster angle. This finding was confirmed not only by our macroscopic observations but also by our numerical simulations.

For configuration 2 (filaments crossed between layers), the K_{IC} values are almost identical for different combinations of raster angles. The order of magnitude of the K_{IC} is 3 $MPa\sqrt{m}$, this value is still lower than for continuous ABS. Indeed, in this type of configuration, only 50% of the layers constituting the specimen that generate a good strength. By analyzing the damage phenomenon of this configuration 2, we observed two types of failures. The first type is the separation of adjacent filaments. In this case, the crack follows the largest raster angle of the structure. Except for the case (45°/-45°), where the crack remains more or less straight but with small bifurcations. The second type corresponds to the transverse rupture of the filament which opposes a resistance somewhat close to that of the continuous ABS.

REFERENCES

[1] Gordelier, T. J., Thies, P. R., Turner, L. and Johanning, L. (2019). Optimising the FDM additive manufacturing process to achieve maximum tensile strength: a state-of-the-art review. Rapid Prototyping Journal.

[2] Goh, G. D., Agarwala, S., Goh, G. L., Dikshit, V., Sing, S. L. and Yeong, W. Y. (2017). Additive manufacturing in unmanned aerial vehicles (UAVs): Challenges and potential. Aerospace Science and Technology, 63, pp. 140-151.

[3] Palanisamy, C. and Raman, R. (2021). Additive manufacturing: a review on mechanical properties of polyjet and FDM printed parts. Polymer Bulletin, pp. 1-52.

[4] Calignano, F., Manfredi, D., Ambrosio, E. P., Biamino, S., Lombardi, M., Atzeni, E., Fino, P. (2017). Overview on additive manufacturing technologies. Proceedings of the IEEE, 105(4), pp. 593-612.

[5] Turner, B. N., Strong, R. and Gold, S. A. (2014). A review of melt extrusion additive manufacturing processes: I. Process design and modeling. Rapid Prototyping Journal.

[6] Yadav, D. K., Srivastava, R. and Dev, S. (2020). Design & fabrication of ABS part by FDM for automobile application. Materials Today: Proceedings, 26, pp. 2089-2093.

[7] Zaldivar, R. J., Witkin, D. B., McLouth, T., Patel, D. N., Schmitt, K. and Nokes, J. P. (2017). Influence of processing and orientation print effects on the mechanical and thermal behavior of 3D-Printed ULTEM® 9085 Material. Additive Manufacturing, 13, pp. 71-80.

[8] Jungivala, D. and Gurrala, P. K. (2021). Finite element analysis of fused filament extrusion build part using different build orientation. Materials Today: Proceedings, 38, pp. 3264-3268.

[9] Mohamed, O. A., Masood, S. H. and Bhowmik, J. L. (2016). Mathematical modeling and FDM process parameters optimization using response surface methodology based on Q-optimal design. Applied Mathematical Modelling, 40(23-24), pp. 10052-10073.

[10] Letcher, T., Rankouhi, B. and Javadpour, S. (2015, November). Experimental study of mechanical properties of additively manufactured ABS plastic as a function of layer parameters. In ASME International Mechanical Engineering Congress and Exposition, 57359, V02AT02A018. American Society of Mechanical Engineers.

[11] Mishra, P. K., Senthil, P., Adarsh, S. and Anoop, M. S. (2021). An investigation to study the combined effect of different infill pattern and infill density on the impact strength of 3D printed polylactic acid parts. Composites Communications, 24, 100605.

[12] Gao, X., Qi, S., Kuang, X., Su, Y., Li, J. and Wang, D. (2021). Fused filament fabrication of polymer materials: A review of interlayer bond. Additive Manufacturing, 37, 101658.

[13] Turner, B. N. and Gold, S. A. (2015). A review of melt extrusion additive manufacturing processes: II. Materials, dimensional accuracy, and surface roughness. Rapid Prototyping Journal.

[14] Lubombo, C. and Huneault, M. A. (2018). Effect of infill patterns on the mechanical performance of lightweight 3D-printed cellular PLA parts. Materials Today Communications, 17, pp. 214-228.

[15] Othmani, M., Chouaf, A. and Zarbane, K. (2017, October). Modeling and numerical analysis of the mechanical behavior of parts obtained by the FDM type additive manufacturing process. In Proceedings of the Mediterranean Symposium on Smart City Application, pp. 1-4.

[16] Sood, A. K., Ohdar, R. K. and Mahapatra, S. S. (2012). Experimental investigation and empirical modelling of FDM process for compressive strength improvement. Journal of Advanced Research, 3(1), pp. 81-90.

[17] Ayatollahi, M. R., Nabavi-Kivi, A., Bahrami, B., Yahya, M. Y. and Khosravani, M. R. (2020). The influence of in-plane raster angle on tensile and fracture strengths of 3D-printed PLA specimens. Engineering Fracture Mechanics, 237, 107225.

[18] Ameri, B., Taheri-Behrooz, F. and Aliha, M. R. M. (2021). Evaluation of the geometrical discontinuity effect on mixed-mode I/II fracture load of FDM 3D-printed parts. Theoretical and Applied Fracture Mechanics, 113, 102953.

[19] Hart, K. R. and Wetzel, E. D. (2017). Fracture behavior of additively manufactured acrylonitrile butadiene styrene (ABS) materials. Engineering Fracture Mechanics, 177, pp. 1-13.

[20] Patel, N. D. and Patel, B. B. (2015). Fracture analysis of fdm manufactured acrylonitrile butadiene styrene using FEM. International Journal of Recent Research in Civil and Mechanical Engineering, 2(1), pp. 84-90.

[21] Li, J., Yang, S., Li, D. and Chalivendra, V. (2018). Numerical and experimental studies of additively manufactured polymers for enhanced fracture properties. Engineering Fracture Mechanics, 204, pp. 557-569.

[22] Majid, F., Zekeriti, N., Lahlou, M. and Mrani, B. (2020). Mechanical behavior and crack propagation of ABS 3D printed specimens. Procedia Structural Integrity, 28, pp. 1719-1726.

[23] Aourik, O., Othmani, M., Saadouki, B., Abouzaid, K. and Chouaf, A. (2021). Fracture toughness of ABS additively manufactured by FDM process. Journal of Achievements in Materials and Manufacturing Engineering, 109(2). DOI: 10.5604/01.3001.0015.6258.

[24] Djouda, J. M., Gallittelli, D., Zouaoui, M., Makke, A., Gardan, J., Recho, N. and Crépin, J. (2020). Local scale fracture characterization of an advanced structured material manufactured by fused deposition modeling in 3D printing. Frattura ed Integrità Strutturale, 14(51), pp. 534-540.

[25] Araújo, H., Leite, M., Ribeiro, A. M. R., Deus, A. M., Reis, L. and Vaz, M. F. (2019). Investigating the contribution of geometry on the failure of cellular core structures obtained by additive manufacturing. Frattura ed Integrità Strutturale, 13(49), pp. 478-486.

[26] ISO 13586 (2018), Plastics - Determination of Fracture Toughness (GIC and K_{IC}) - Linear Elastic Fracture Mechanics (LEFM) Approach, International Organization for Standardization, Geneva, Switzerland.

[27] ASTM D5045, Standard Test Methods for Plane-Strain Fracture Toughness and Strain Energy Release Rate of Plastic Materials, ASTM International, West Conshohocken, PA, 1999, DOI: 10.1520/D5045-99.

[28] H. Tada, (2000). The analysis of cracks handbook, New York: ASME Press, 2, 1.

[29] Oskui, A. E. H., Choupani, N. and Haddadi, E. (2014). Experimental and numerical investigation of fracture of ABS polymeric material for different sample's thickness using a new loading device. Polymer Engineering & Science, 54(9), pp. 2086-2096.

[30] Khatri, A. and Adnan, A. (2016, November). Effect of raster orientation on fracture toughness properties of 3D printed ABS materials and structures. In ASME International Mechanical Engineering Congress and Exposition, 50633, V009T12A064. American Society of Mechanical Engineers.

[31] Othmani, M., Zarbane, K. and Chouaf, A. (2020). Enhanced Mesostructural Modeling and Prediction of the Mechanical Behavior of Acrylonitrile Butadiene Styrene Parts Manufactured by Fused Deposition Modeling. International Review of Mechanical Engineering (IREME), 14(4), 243.

[32] Schmailzl, A., Amann, T., Glockner, M. Fadanelli, M. Wagner, M., Hierl, S. (2012). Finite element analysis of thermoplastic probes under tensile load using LS-DYNA compared to ANSYS WB 14 in correlation to experimental investigations, Proceedings of the ANSYS Conference & 30th CADFEM users' meeting, Kassel.